UV-Curing Additive Manufacturing of Bio-Based Thermosets: Effect of Diluent Concentration on Printing and Material Properties of Itaconic Acid-Based Materials

ACS OMEGA

http://pubs.acs.org/journal/acsodf

Article

UV-Curing Additive Manufacturing of Bio-Based Thermosets: Effect of Diluent Concentration on Printing and Material Properties of Itaconic Acid-Based Materials

Lazaros Papadopoulos, Lorenzo Pezzana, Natalia Maria Malitowski, Marco Sangermano, Dimitrios N. Bikiaris,* and Tobias Robert*

Cite This: *ACS Omega* 2023, 8, 31009−31020

Read Online

ACCESS | Metrics & More | Article Recommendations | Supporting Information

ABSTRACT: In the quest toward sustainable thermosets, research has been conducted on various polymer classes like epoxy, benzoxazines, acryl-/methacrylates, etc. One particular group that can also be utilized as sustainable inks for additive manufacturing is itaconic acid-based unsaturated polyester resins. However, due to increased viscosity of the resins, the use of reactive diluents is required to increase their processability. While research has focused on creating different polymeric structures to expand the possible applications, the required amount of diluent has not received equal attention. In this work, a group of itaconic acid-based polyesters was synthesized to create a series of formulations with different reactive diluent contents. The physicochemical properties of the prepared formulations, along with their reactivity toward UV light, were assessed via photo-differential scanning calorimetry (photo-DSC), real-time attenuated total reflectance (RT-ATR), and photorheology measurements. The same formulations were then used to fabricate test specimens via digital light processing (DLP) three-dimensional (3D) printing, which were examined as to their thermomechanical properties by means of dynamic mechanical analysis (DMA) and thermogravimetric analysis (TGA) measurements.

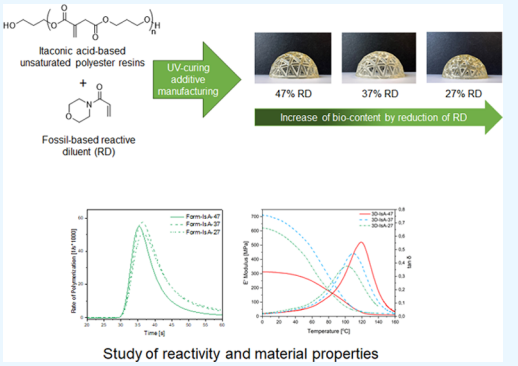

INTRODUCTION

Plastic materials dominate today's society due to their versatility and low cost, substituting the use of traditional materials like wood, steel, and glass. However, the extensive use of polymer-based products comes with a high environmental burden, as recycling rates of these materials are very low and a major fraction ends up in landfills or even worse in the environment. In addition, the vast majority of commercial plastics is produced from depleting nonrenewable feedstock.[1,2] As the environmental awareness of the public keeps increasing so does the demand for more sustainable materials that can address these challenges. One way to reduce the dependency on fossil fuels is the use of monomers from renewable resources as polymeric precursors.[3]

In that regard, itaconic acid is a promising monomer that needs to be highlighted. Back in 2004, it was included in a study published by the US Department of Energy, with the top 12 most promising bio-based monomers.[4] Since then, it has evolved into an intensively studied platform molecule, from which a variety of materials can be prepared. Compared to other bio-based monomers, it has the advantage of being already produced on an industrial scale at a competitive price. More specifically, over 80 ktons/a is produced via sugar fermentation by the fungus *Aspergillus terreus* and the price is less than 2 €/kg.[5−7] In addition, itaconic acid has the advantage to be very versatilely applicable. First, it is considered as an alternative to maleic acid in bio-based unsaturated polyester resins for thermosetting applications.[8−13] In this respect, recent studies have shown that the utilization of itaconic acid in these applications results in the reduction of greenhouse gas emissions and of the total energy consumption.[14] Second, the external double bond exhibits a higher reactivity toward radical reactions compared to the internal double bond of the maleic acid. Therefore, several studies focused on the use of itaconic acid as an alternative to (meth)acrylic acid. For example, itaconic acid can be used to create homopolymers and copolymers through radical polymerization reactions.[15−17] In addition, monoesters of itaconic acid have been used as an alternative to acrylic acid in the reaction with epoxidized vegetable oils.[18,19] Furthermore, polyesters from itaconic acid can also be used as oligomers for UV-curing applications, such as coatings,[13,20,21]

Received: April 24, 2023
Accepted: July 19, 2023
Published: August 15, 2023

printing inks,[22] and materials for additive manufacturing (AM) (three-dimensional, 3D printing).[23−25] The latter is especially interesting as bio-based materials for additive manufacturing are still scarce, as usually materials derived from acrylic acid are being utilized.[26−30] One of the challenges associated with additive manufacturing (AM) processes is the need for low-viscosity materials. This is usually achieved by creating formulations from oligomers with high amounts (up to 60%) of monomeric reactive diluents. In many cases esters from acrylic acid or acrylamides are used. Therefore, in order to be able to increase the overall bio-based content of AM materials two approaches can be followed: One possibility is the use of a combination of bio-based oligomers with bio-based diluents. Recently, we were able to show that the combination of itaconic acid-based polyesters with the bio-based diluent isobornylacrylate (IBOA) results in AM formulations with an overall bio-content of 85%.[31] However, in this case, not all polyesters were able to form homogeneous formulations with this diluent and acryloyl morpholine (ACMO), a diluent from petrochemical resources, had to be used to be able to print these materials. As acrylic acid itself is not commercially available from renewable resources, we also investigated the use of itaconic-derived reactive diluents.[32] The resulting formulations were the first example of (meth)acrylic acid-free AM materials. However, due to the lower reactivity of itaconic acid, longer printing time was needed to obtain materials with satisfying properties.

Another possible option to increase the overall bio-based content of AM formulations is the reduction of the amount of the petro-based reactive diluent. However, the challenge here is that the resulting formulations are still processable on standard AM machines. Therefore, we herein investigate the influence of the step-wise reduction of ACMO in AM formulations with itaconic acid-based oligomers. For this, five new polyester itaconates with a high-density of radical cross-linking groups were synthesized to ensure sufficient cross-linking of the materials even at lower percentages of reactive diluent. In addition, monomers of different structures (aromatic, aliphatic) were incorporated in each polyester oligomer to examine if they could influence the properties of the final materials. Three different reactive diluent concentrations were selected, and formulations were examined regarding the evolution of viscosity and reactivity toward UV light. Real-time attenuated total reflectance (ATR) and photorheology assays of itaconic acid-based formulations are reported within for the first time. Finally, additive manufacturing assays were performed, and the thermomechanical properties of the cross-linked materials were investigated to determine the influence of reactive diluent concentration on their properties.

MATERIALS AND METHODS

Materials. Itaconic acid (IA, 99%), succinic acid (SA, 99%), sebacic acid (SebA, 99%), isophthalic acid (IsA, 99%), and phthalic anhydride (PhA, 99%) were purchased from Merck, Darmstadt, Germany. 2,5-Furandicarboxylic acid (FDCA, 97%) was purchased from Biosynth, Bratislava, Slovakia. Chloroform-d_1 (99.8% D) + 0.03% TMS v/v was obtained from Carl Roth, Karlsruhe, Germany. 2,6-Di-*tert*-butyl-4-methylphenol (BHT, 99%) was bought from Merck, Darmstadt, Germany. 4-Methoxyphenol (MeHQ, 99%) was purchased from Sigma-Aldrich Chemie, Steinheim, Germany. 1,3-Propanediol (PDO, 99.7%) was kindly provided by DuPont Tate & Lyle Bio Products, Loudon, NH. FASCAT 4101 catalyst was kindly provided by PMC Group, Mount Laurel, NJ. Acryloyl morpholine (ACMO, 99%) was purchased from Rahn GmbH, Frankfurt, Germany. Diphenyl(2,4,6-trimethylbenzoyl)phosphine oxide (TPO) was purchased from IGM Resins. Solvents were reagent or analytical grade and were purchased from VWR International, Fontenay-sous-Bois, France. All reagents were used without further purification.

Polyester Synthesis. Five unsaturated polyesters were synthesized via direct esterification of itaconic acid, PDO, and a secondary acid. A diacid to diol ratio of 1:1.45 was used. As an example, the synthesis of 400 g of PE-SebA is described. 107.3 g (0.3 equiv, 0.53 mol) of SebA, 161 g (0.7 equiv, 1.24 mol) of IA, and 195.1 g (1.45 equiv, 2.56 mol) of PDO were charged into a three-necked round-bottom flask, along with 0.12 g (0.06 wt %) of MeHQ, 0.16 g (0.08 wt %) of BHT, and 1.56 g (0.39 wt %) of FASCAT 4101. The flask was equipped with a Dean−Stark condenser, a mechanical stirrer, and an immersed thermocouple to control the temperature of the heating mantle. Water removal was facilitated by the addition of toluene (10% w/w). The mixture was heated gradually until homogenization and then temperature was increased to 180 °C until an acid value (AV) of <5 mg KOH/g was reached (usually 3−4 h). The toluene was then removed under reduced pressure at 130 °C and 100 mg of MeHQ was added to the resin for stabilization. The polyesters were obtained without further purification as transparent viscous, slightly yellow to light brown liquids, depending on their composition. The description of resin compositions is given in Table 1.

Table 1. Composition of the Synthesized Polyesters and Bio-Based Content

sample	IA (equiv)	secondary acid (equiv)	PDO (equiv)	DBD[a] (mmol/g)	bio-based content[b] (wt %)
PE-SebA	0.7	0.3	1.45	3.1	100
PE-IsA				3.3	80
PE-SA				3.5	100
PE-FDCA				3.3	100
PE-PhA				3.3	82

[a]Double-bond density. [b]% of mass of renewable monomers used for the synthesis of each resin.

Measurements. Fourier transform infrared (FTIR) spectra of the synthesized resins were obtained on a Thermo Scientific Nicolet iS5 FTIR (Thermo Fisher Scientific, Waltham, MA) using the ATR technique (32 scans, resolution of 4 cm^{-1}). The photocuring process of the formulations was followed in real time by means of a Nicolet iS 50 spectrometer. The formulations were spread on a silicon substrate, using a film bar to produce films of 12 μm. The visible light source was a Lightningcure LC8 (Hamamatsu Photonics, Hamamatsu, Japan), which was directed on the sample with an optic fiber. Spectra were collected with a resolution of 4 cm^{-1} in real-time mode, and the data were processed by OMNIC software, developed by Thermo Fisher Scientific. The signal at 790 cm^{-1} corresponding to the C═C bond of ACMO was monitored, while the signal at 1730 cm^{-1} corresponding to the C═O bond of the ester was used as a reference.

NMR experiments were conducted on a Bruker Avance III 400 MHz spectrometer (Bruker, Billerica, MA). ^{1}H NMR

https://doi.org/10.1021/acsomega.3c02808
ACS Omega 2023, 8, 31009−31020

Scheme 1. Synthetic Pathway for the Materials of the Study

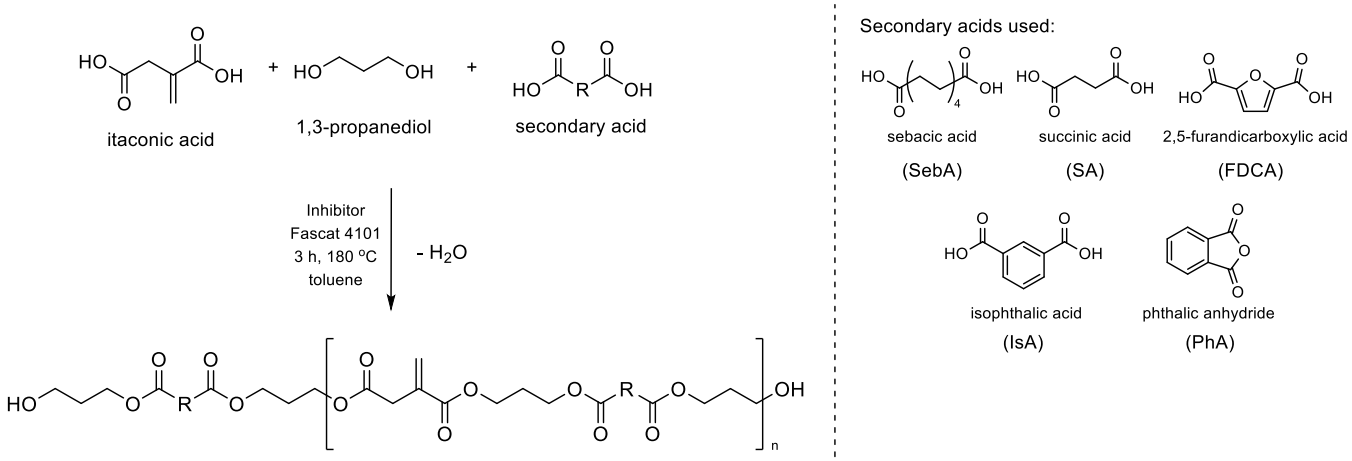

shifts of polymers are reported in ppm (δ) downfield from tetramethylsilane (TMS) and were determined by reference to the residual solvent peak (chloroform-d_1, 7.26 ppm for hydrogen atoms).

The acid value (AV) is proportional to the unreacted acid groups. It was defined as the milligram of KOH required to neutralize one gram of sample and was determined according to DIN EN ISO 2114 by titrating the carboxylic acid groups of the sample with potassium hydroxide solution in methanol (0.3 mol/L). The sample (1−2 g) taken was dissolved in acetone.

Determination of the molar mass distribution was performed by size exclusion chromatography (SEC) measurements with tetrahydrofuran as an eluent and with polystyrene calibration in the range of 162−70,000 g/mol. Three SDV 1000A columns at 40 °C, a variable UV detector (here: 254 nm), a refractive index detector, and the software (WinGPC Unity) were provided by Polymer Standard Service (Mainz, Germany). The samples were filtered over a 0.2 mm poly(tetrafluoroethylene) (PTFE) filter before injection.

Viscosity measurements were performed on a Malvern Kinexus lab + (Malvern Panalytical Ltd, Malvern, U.K.) equipped with a cone−plate geometry (CP 4°, 40 mm). Measurements were made with a rotation speed of 100 s^{-1} for 10 s. Five measurements were made at each temperature, and the average value was calculated.

Photo-differential scanning calorimetry (Photo-DSC) measurements were conducted on a DSC^{3+} (Mettler-Toledo, Greifensee, Switzerland) equipped with a Lightningcure LC8 UV spotlight source (Hamamatsu Photonics, Hamamatsu, Japan) at 70% of its intensity. To get the integration of the heat of reaction, two runs were carried out with a short break between the runs to let the resin cool down. The second run was made once the material was fully cured and the baseline was stable. Then, the second curve was subtracted from the first to obtain the curve related to the curing only. Each run is conducted as follows: 30 s at the set temperature (25, 40, or 60 °C, respectively, at atmospheric pressure under nitrogen) without the lamp; then, the lamp is turned on for 4.5 min. The break between the runs lasts 30 s.

Photorheology data were collected by means of an Anton Paar302MC rheometer (PhysicaMCR302, Graz, Styria). The rheometer was set with a plate−plate geometry, the outside diameter of the metal disk was 25 mm and a glass disk was used as a bottom support in order to guarantee the irradiation of the sample. The distance between the two disks was set at 200 μm. The visible light was provided by optic fibers to directly irradiate the sample. A Hamamatsu Lightningcure LC8 was used as a visible light source with a light intensity of about 40 mW/cm^2 provided on the surface of the sample. The lamp was turned on after 60 s of stabilization and the measurements were performed in the oscillatory condition at a frequency of 1 Hz, with strain 1% and in isothermal condition at room temperature.

Additive manufacturing experiments were conducted on a Phrozen Sonic 4K DLP printer equipped with a 50 W UV LED array (405 nm). The samples were cured with a layer thickness of 20 μm and an exposure time of 3 s per layer for all formulations. Approximately 40 g of formulation was used to print five rectangle specimen at once, suitable for dynamic mechanical analysis (DMA) measurements. The print orientation of the samples was 0°. After the process, samples were removed from the printer and post-cured in a post-curing light oven (Wanhao Boxman-1) for 30 min. The samples were turned after 15 min to ensure even curing of the specimens.

Dynamic mechanical analysis (DMA) was carried out on a Tritec 2000 DMA (Triton Technology, Loughborough, U.K.) in single cantilever bending mode. Measurements were performed on the rectangle bars (25 × 10 × 4 mm) which were prepared with additive manufacturing. Samples were studied under nitrogen in a temperature range of 0−150 °C (2 K/min, 1 Hz, maximum displacement 0.01 mm). The exact dimensions of specimens were determined before each experiment, and five test bars were measured for each sample. The cross-linking density of the cross-linked materials was evaluated according to the kinetic theory of rubber elasticity:[33]

$$\nu = \frac{E'}{3RT}$$

where E' is the storage modulus in the rubbery plateau region at $T = T_g + 30$ °C, R is the gas constant, and T is the absolute temperature in K.

Thermogravimetric analysis (TGA) of cured resins was performed on a TGA/DSC 1 (Mettler-Toledo, Greifensee, Switzerland) under nitrogen (35 mL/min). Samples of ca. 10 mg were heated from 25 to 700 °C with a heating rate of 10 K/min.

https://doi.org/10.1021/acsomega.3c02808
ACS Omega 2023, 8, 31009−31020

RESULTS AND DISCUSSION

In the course of this study, five polyesters were synthesized by means of azeotropic polycondensation. Besides 0.7 equiv of itaconic acid (IA) and 1.45 equiv of 1,3-propanediol (PDO), 0.3 equiv of a second diacid was used as a building block to examine the effect of different aliphatic and aromatic diacids on the polyester resins (Scheme 1). The exact compositions are listed in Table 1. The excess of PDO was chosen to obtain resins with viscosities suitable for additive manufacturing. As mentioned in the Introduction section, the goal was to examine how the ratio between the resin and the reactive diluent influenced the key characteristics of formulations like viscosity and reactivity, and to investigate whether those characteristics translated into materials with different properties after the cross-linking phase. Therefore, the polymeric structure was designed to be rich in itaconic acid moieties to allow a better "interaction" between the resin and the diluent. PDO was selected as a short "spacer" between the C=C double bonds and the remaining acid moieties were selected to achieve different physicochemical properties of the polymers.

Structural Characterization. *FTIR.* The structure of the synthesized resins was preliminarily assessed with ATR spectroscopy. The spectra are depicted in Figure 1. The

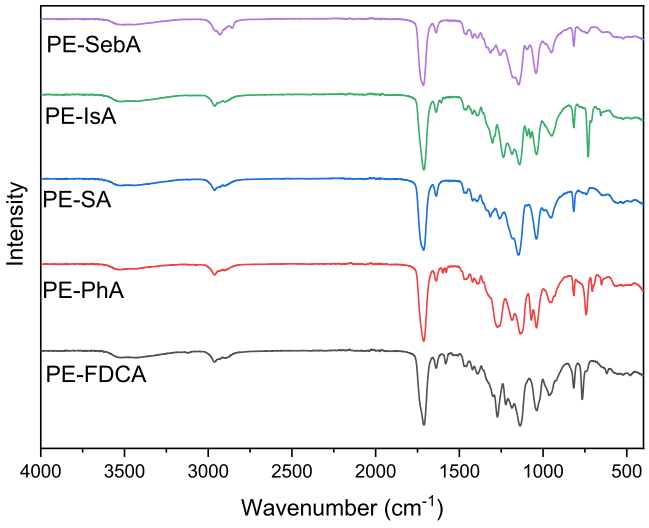

Figure 1. ATR spectra of the polyesters prepared in the course of this study.

most significant vibrations for these polyesters are the C=O stretching vibrations of the ester bond, represented by the signal at 1730 cm^{-1}, and the C=C deformation and C=C stretch vibrations, represented by the signals at 810 and 1640 cm^{-1}, respectively. As a diol excess was used during synthesis, a broad signal derived from the −OH end groups is also visible at 3500 cm^{-1}. Finally, there are also signals that are unique for each material, as different secondary acids were used, e.g., ring vibrations from aromatic monomers are visible at 1600 cm^{-1}.

NMR. The NMR spectra of the synthesized resins are presented in Figure 2. In the ^1H NMR spectra, the characteristic resonance signals of the itaconate units are observed at 5.7 and 6.3 ppm (=CH_2 group) and around 3.3 ppm (−$CH_2C(O)$ group). There are no signals indicating isomerization of itaconic to mesaconic acid;[34] therefore, the C=C remains in the exo position, which is necessary for a sufficient reactivity in subsequent UV-induced cross-linking. For the propanediol segments, peaks attributed to the $C(O)OCH_2$− groups are observed around 4.1−4.6 ppm, depending on the type of secondary acid, while the central −CH_2− shows in the 1.5−2.5 ppm region. Finally, the characteristic peaks of each secondary acid are visible in the respective spectra. A more detailed assignment of the signals is given in the Supporting Information.

Physicochemical Characterization. Moving to the physicochemical characterization of the resins, SEC results are shown in Figure 3. A Gaussian distribution of the molecular weight is observed, which is characteristic for polycondensation polymers. As the structure of the resins is quite similar, the obtained curves are practically overlapping and the molecular weights of the resins are in the same range, from 1020 to 1130 g/mol. Furthermore, no high-molecular-weight fraction can be observed in the elugrams. These findings in combination with dispersities below 2 are strong indications that no cross-linking or Ordelt side reactions did occur during the synthesis.

In Figure 4, the DSC scans of the polyesters are shown. While similar resins in our previous work[31] exhibited glass-transition temperatures in the range of <−50 °C up to 13.5 °C, this set of polymers had only a narrow range of the T_g, with a maximum T_g of −28 °C for PE-PhA. This exhibits the reduced influence of the secondary acid on the properties of the materials, as it is limited to 0.3 equiv of total acid used. The SEC and DSC results are summarized in Table 2.

Formulations. Polymers designed for UV-curing AM are often mixed with reactive diluents to create formulations with a proper viscosity to be processable in the 3D printer. In addition, diluents can alter both the reactivity toward UV light and the final properties of the cured material. In our previous study,[31] we were able to show that the structure of the polyester had a significant influence on the behavior of the formulation, as lower viscosities and flexible structures lead to higher conversions and better thermomechanical properties of the 3D-printed materials. However, it is also important to determine the influence of the amount of reactive diluent on the properties of the formulation and the subsequently fabricated materials. Therefore, we created formulations based on the above-described polyesters, with three different concentrations of ACMO, to examine the effect on the printing process and the thermomechanical properties of the cured material. The behavior of the formulations was studied regarding viscosity and reactivity toward UV light, which is significantly altered by the step-wise reduction of ACMO in the formulation. Finally, we examined the properties of the formulations with the lowest amount of ACMO under three different temperatures. The composition of the formulations, their bio-based content, their viscosity, and the results of the photo-DSC are summarized in Table 3.

As anticipated, the reduction of the reactive diluent increased the viscosity of the formulations. For resins containing aromatic monomers, this phenomenon was more pronounced, due to the higher rigidity of their chemical structure and in turn the higher initial viscosity of the neat resin. Interestingly enough, the reduced mobility of the systems had a positive effect regarding the conversion of the C=C double bonds, at least initially. A 10% reduction of the amount of reactive diluent led to increased conversions for all systems, as listed in Table 3. To explain this phenomenon, the progression of the polymerization rate must be examined. For this, the rate of polymerization was plotted against time

https://doi.org/10.1021/acsomega.3c02808
ACS Omega 2023, 8, 31009−31020

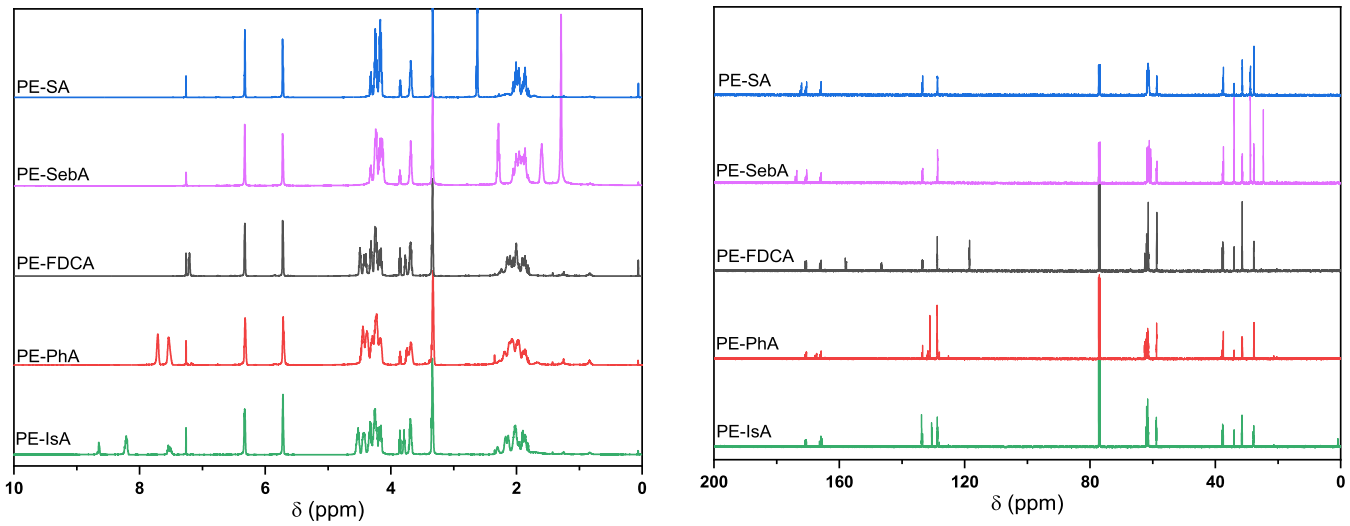

Figure 2. NMR spectra of the synthesized polyesters.

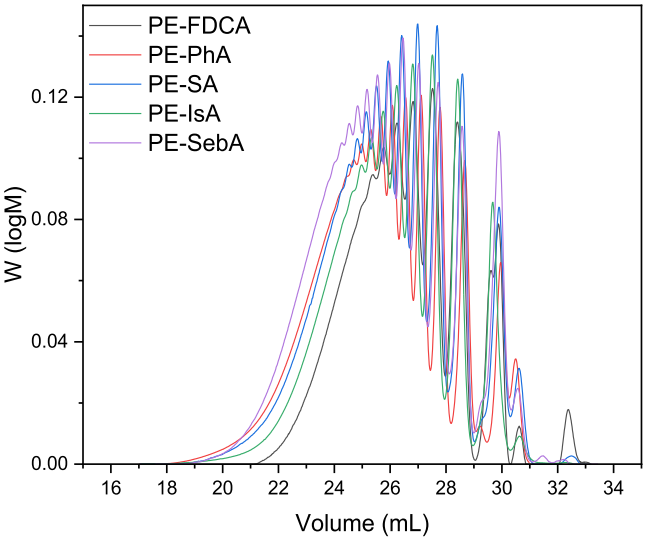

Figure 3. SEC elugrams of the synthesized polyesters.

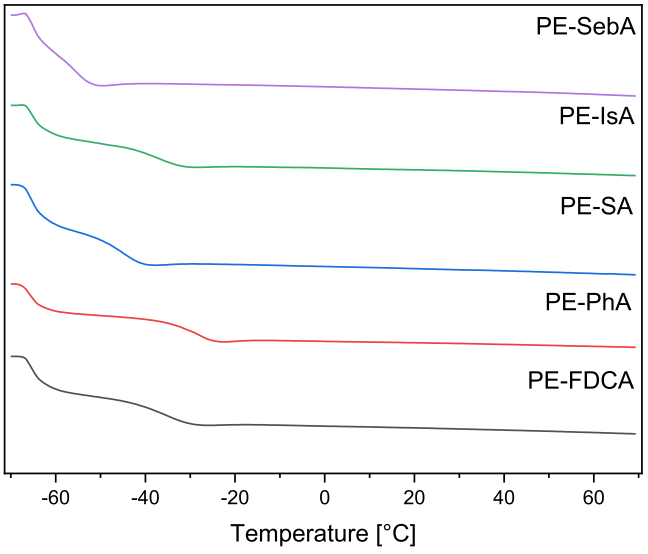

Figure 4. DSC scan of the prepared resins.

Table 2. Glass-Transition Temperature and Molecular Weight of the Prepared Materials

sample	M_n (g/mol)	M_w (g/mol)	$Đ$	T_g (°C)
PE-SebA	1070	2130	1.99	<−50
PE-IsA	1070	1850	1.74	−36
PE-SA	1020	1970	1.94	−45
PE-FDCA	1020	1700	1.67	−35
PE-PhA	1130	2220	1.96	−28

(Figure 5a) and against C═C conversion (Figure 5b). It is shown that the maximum rate of polymerization (ROP_{max}) is reached earlier for formulations with 47% ACMO compared to formulations with 37% ACMO. However, then the polymerization slows down and stops at lower conversions for formulations with 47% diluent, while for formulations with 37% diluent the cross-linking is prolonged and higher conversions are reached. It is known that the final conversion is influenced by viscosity-assisted reaction diffusion in the autodeceleration step.[35] Therefore, the gelation point is reached earlier for formulations with 47% ACMO. However, since they present lower initial viscosity, this behavior must be derived from their composition. Indeed, ACMO contains an acrylic acid-derived C═C, which has a higher reactivity compared to the itaconic acid-derived C═C of the polyester resins. The high concentration of ACMO for formulations with 47% diluent implies that during the propagation phase of cross-linking, there is a higher chance of those small and mobile radicals to react with each other, therefore reducing the overall mobility of the system early and limiting the overall C═C conversion. For formulations with 37% diluent, there is enough ACMO to effectively reduce the viscosity of the system and prolong the propagation stage of the polymerization, but not enough to reach the gelation point as early as in the case of 47% ACMO. Therefore, gelation is delayed compared to formulations with 47% ACMO and significantly higher conversions are reached. Finally, for formulations with 27% ACMO, the viscosity of the system is significantly higher compared to the other two. The ROP_{max} is the most affected parameter by this increase, being lower for all samples when compared with formulations of 37% diluent. Despite that, overall C═C conversion is similar between the two groups, as gelation time is again prolonged at lower ACMO concen-

https://doi.org/10.1021/acsomega.3c02808
ACS Omega 2023, 8, 31009−31020

Table 3. Properties of the Prepared Formulations

formulation	resin	reactive diluent	viscosity@20 °C (Pa·s)	bio-based content[a]	DBD (mmol/g)	RoP_{max}[b] ($s^{-1} \times 10^3$)	C %[c]
Form-SebA-47	PE-SebA	47% ACMO	0.23	50	4.88	60.2	65
Form-SebA-37		37% ACMO	0.44	60	4.48	70.2	84
Form-SebA-27		27% ACMO	0.74	70	4.08	53.8	80.5
Form-SebA-27@40 °C			0.19		4.08	63.2	87.8
Form-SebA-27@60 °C			0.07		4.08	69.4	89.6
Form-IsA-47	PE-IsA	47% ACMO	0.44	40	4.98	54.9	54.6
Form-IsA-37		37% ACMO	1.27	48	4.6	57.6	73.5
Form-IsA-27		27% ACMO	3.03	56	4.22	50.7	70.6
Form-IsA-27@40 °C			0.48		4.22	65.9	79.5
Form-IsA-27@60 °C			0.13		4.22	74.3	82.1
Form-SA-47	PE-SA	47% ACMO	0.3	50	5.08	70.4	69.3
Form-SA-37		37% ACMO	0.65	60	4.72	54	73.6
Form-SA-27		27% ACMO	1.21	70	4.36	46.4	75
Form-SA-27@40 °C			0.24		4.36	51.1	78.8
Form-SA-27@60 °C			0.08		4.36	69.1	82.4
Form-FDCA-47	PE-FDCA	47% ACMO	0.51	50	4.98	59.9	68.5
Form-FDCA-37		37% ACMO	1.34	60	4.6	48.6	69.8
Form-FDCA-27		27% ACMO	4.69	70	4.22	34.1	59.2
Form-FDCA-27@40 °C			0.65		4.22	42.3	67.4
Form-FDCA-27@60 °C			0.16		4.22	44	70.8
Form-PhA-47	PE-PhA	47% ACMO	0.58	41	4.98	48.8	49.7
Form-PhA-37		37% ACMO	1.72	49.2	4.6	52.5	69.5
Form-PhA-27		27% ACMO	5.14	57.4	4.22	44.4	71.7
Form-PhA-27@40 °C			0.73		4.22	64.6	78.1
Form-PhA-27@60 °C			0.18		4.22	78	82.7

[a]Overall bio-based content of the final formulations. [b]Rate of polymerization (ROP). [c]Double-bond conversion %.

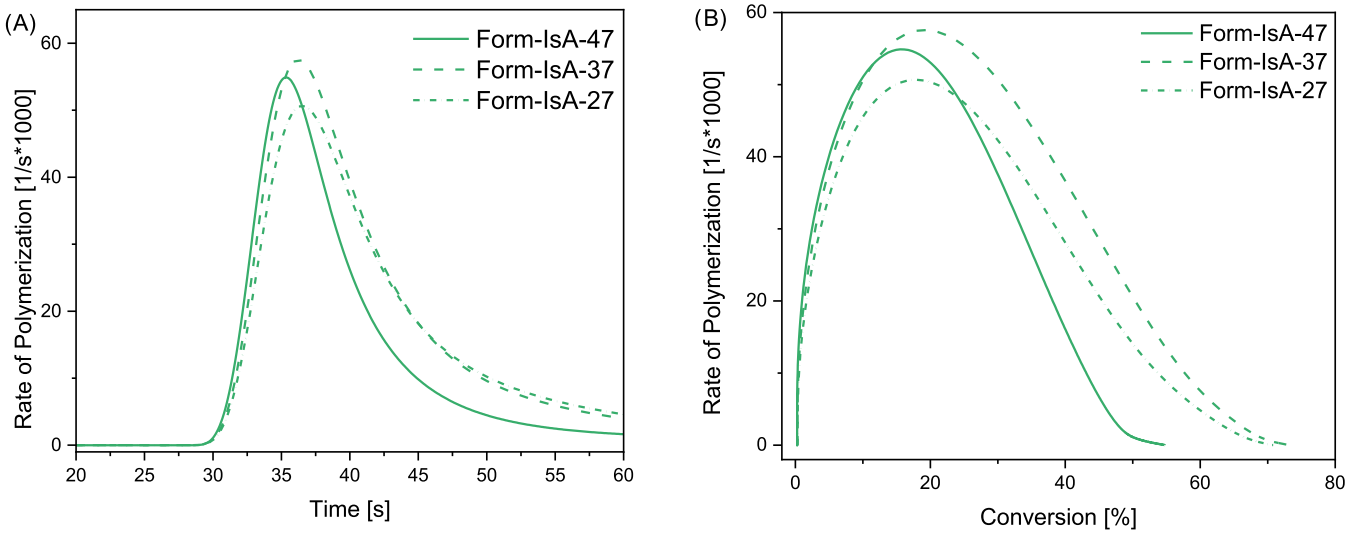

Figure 5. Evolution of the rate of polymerization with reactive diluent alteration (a) vs time and (b) vs double-bond conversion.

trations. Thermograms for the rest of the resins are reported in the Supporting Information, Figure S1.

In a second set of experiments, the effect of temperature on the reactivity toward UV-light-induced polymerization was investigated. Results are given in Figure 6. Formulations with 27% ACMO were selected, as they presented the slowest polymerization rates at room temperature. The increased temperatures lowered the viscosity of the formulations, allowing for an increased mobility of the systems, which translated to increased C=C conversion. For example, for Form-PhA-27, the ROP_{max} was increased from 44.4 $s^{-1} \times 10^3$ ambient to 64.6 $s^{-1} \times 10^3$ at 40 °C and 78 $s^{-1} \times 10^3$ at 60 °C, which actually surpassed the value of Form-PhA-47. In addition, the ROP_{max} was reached earlier during the measurements. These results suggest that, besides reactive diluent concentration, polymerization temperature also has a significant role on the total C=C conversion of these systems, and therefore, it could potentially affect the thermomechanical properties of the materials that were cross-linked under these conditions.

Real-Time ATR. To verify the hypothesis discussed in the previous section, that is, the high reactivity of ACMO is the factor that leads to early gelation and thus to lower conversions, RT-ATR was exploited to monitor the cross-

https://doi.org/10.1021/acsomega.3c02808
ACS Omega 2023, 8, 31009−31020

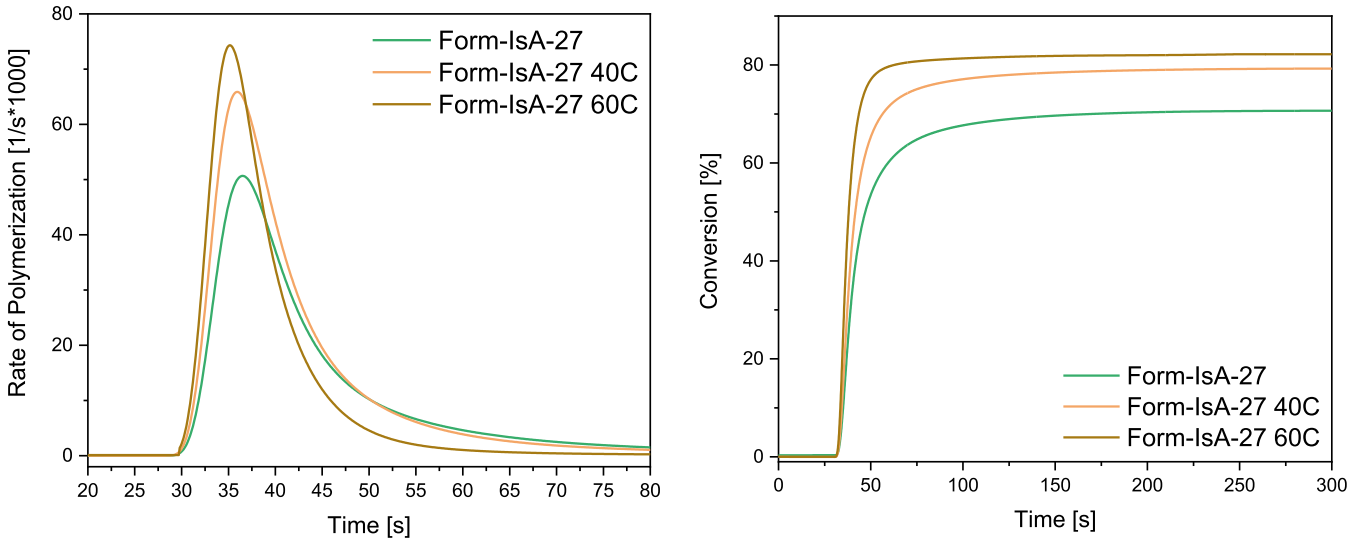

Figure 6. ROP evolution (left) and conversion (right) under increased temperature conditions.

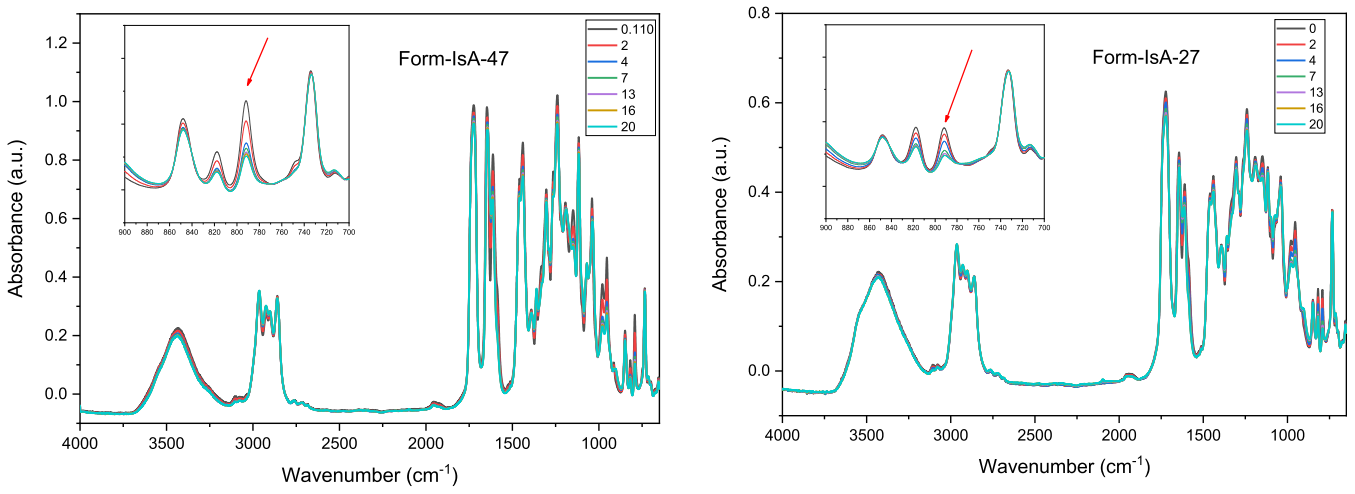

Figure 7. RT-ATR spectra of formulations Form-IsA-47 (left) and Form-IsA-27 (right).

linking reaction. For this, the evolution of the signal at 790 cm^{-1}, corresponding to C═C deformation vibration of the acrylic double bond of ACMO, was followed through time for the different types of formulations. In Figure 7, the real-time IR spectra of formulations Form-IsA-47 and 27 during UV-induced cross-linking are shown. For Form-IsA-47, a steep decrease of the peak area is observed in the initial steps of polymerization, but the rate drops significantly at the later stages. As the content of ACMO is reduced, the rate at which the signal is diminished slows down, being more evenly distributed during the monitoring period. To illustrate this, the area of the signal at 790 cm^{-1} was plotted against time in Figure 8 for formulations Form-IsA, while the rest of the samples are presented in the Supporting Information. It was found that, regardless of the polyester used, formulations with a lower ACMO content have slower polymerization rates in the initial phase of cross-linking, thus verifying the assumptions that were made during the discussion of photo-DSC results.

Photorheology. To further confirm the data obtained from photo-DSC, as well as real-time IR, photorheology measurements were also conducted. The obtained results are presented in Figure 7 and in the Supporting Information. The amount of reactive diluent was found to be the primary parameter that influenced the reactivity of the formulations. In accordance with the results from photo-DSC, formulations containing 47% of ACMO were the fastest ones to start cross-

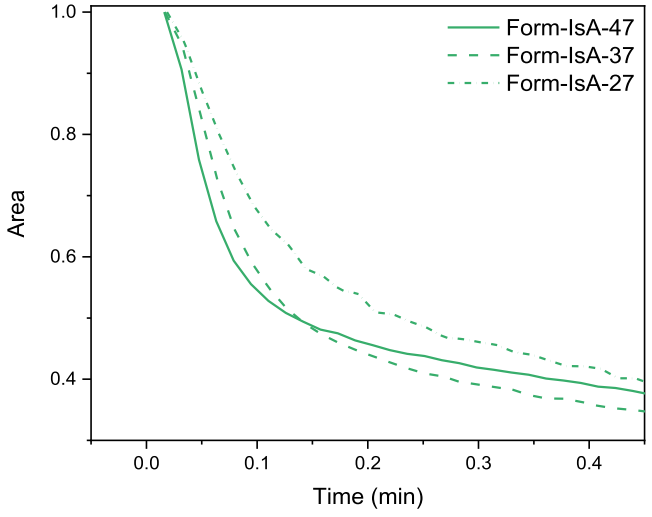

Figure 8. Area evolution over time for formulations Form-IsA.

https://doi.org/10.1021/acsomega.3c02808
ACS Omega 2023, 8, 31009−31020

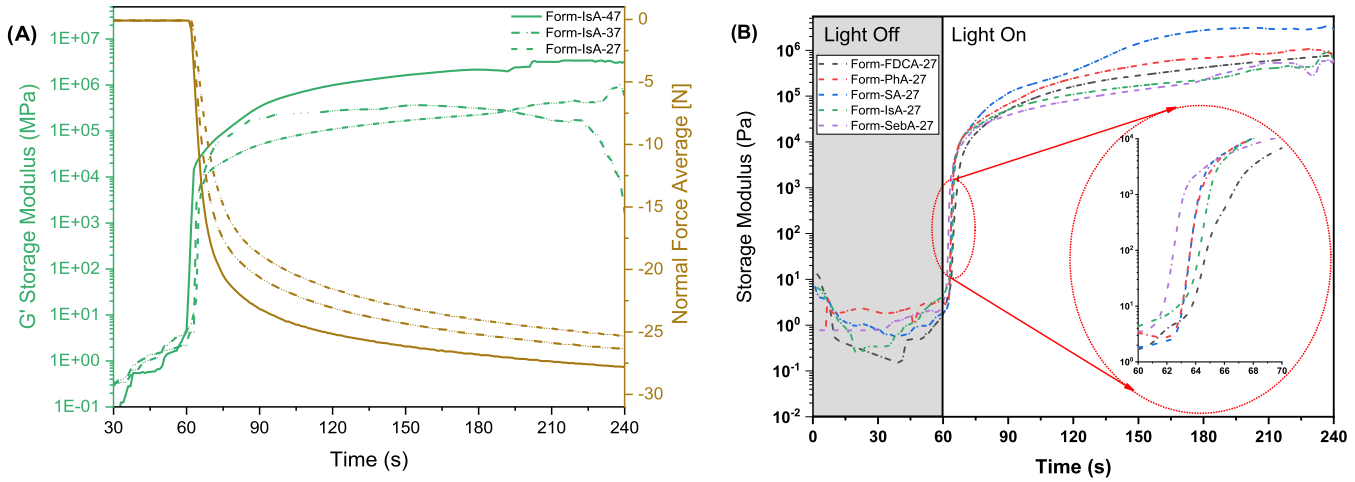

Figure 9. (a) Storage modulus and normal force evolution over time for samples Form-IsA-47, 37, and 27. (b) Storage modulus over time for samples containing different resins and 27% ACMO.

linking. Then, as the amount of reactive diluent was lowered so was the reactivity of the formulations.

Another interesting parameter that was extracted from the photorheology measurements was the evolution of normal force over time. As the space between the rotating disk and the glass substrate has to be kept constant during the measurement, the instrument has the ability to measure the required force to maintain that distance. Furthermore, this "normal force" has been associated with shrinkage phenomena induced by radical polymerization.[36] As shown in Figure 9a, formulations with 47% of ACMO require the highest normal force (in absolute value), therefore indicating the highest shrinkage.[37] This behavior could be explained by the fact that acrylates are known to shrink during polymerization to a higher extent compared to itaconic acid-based materials. The normal force is reduced for formulations of 37% reactive diluent, and then further for those with 27%, regardless of the structure of the resin, supporting this suggestion.

Finally, we compared the behavior of formulations containing 27% ACMO in an effort to highlight the difference of reactivity between the synthesized polyesters and to assess their printability for additive manufacturing purposes (Figure 9b). It was found that the highest induction time before the start of the polymerization was required for the FDCA-containing resin, while the resin-containing SebA required the lowest. This can be explained from the structural mobility of the polyesters, as the "stiffer" aromatic one displayed reduced reactivity. However, it is important to underline that for all formulations, less than 10 s of light exposure was required to reach a steady state (upper plateau) which signals competition of the reaction and the formation of a self-standing layer. This is a direct indication for the printability of the formulations in hand, in ambient conditions, without the need for temperature-assisted additive manufacturing that is employed for other formulation types.[38,39]

Printed Materials. After conducting the abovementioned set of experiments on the formulations, it was clear that their reactivity was adequate for additive manufacturing assays. First, DMA specimens were printed to characterize the properties of the cured materials. A DLP 3D printer was employed, as it offers significantly lower printing times compared to its SLA counterpart. All formulation could be printed with an irradiation time of 3 s per layer. Finally, more complex parts were printed to examine whether bigger and more detailed objects could be manufactured utilizing the formulations prepared in the course of this study. Two different structures were chosen as test objects: one spherical dome and crystal-shaped object. In both cases, the object could be printed without the use of any support structures. However, when formulations with only 27% of ACMO were printed, a longer irradiation time of 10 s per layer had to be used to obtain a satisfying printing result. The printed objects from formulations Form-SA-27 to 47 are shown in Figure 13. The dimensions of the crystal are 4 cm in height and 3 cm in diameter, while the dome exhibits a height of 3 cm and a diameter of 4 cm with a width of the individual bars of 2.5 mm.

DMA. In Figure 10, E' modulus and tan δ evolution of printed materials from resin PE-IsA with different ACMO

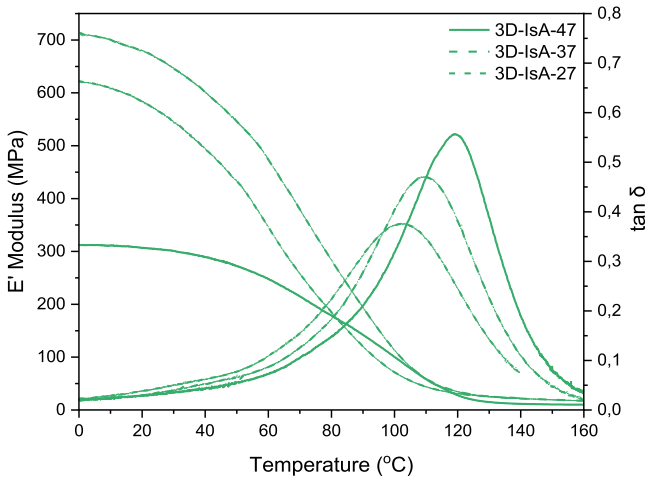

Figure 10. E' modulus and tan δ of materials 3D-IsA-47, 3D-IsA-37, and 3D-IsA-27.

percentages are presented. The respective data for all materials are presented in Table 4 and the rest of the curves are reported in the Supporting Information in Figure S4. Glass-transition temperatures range from 85 °C up to 118 °C, values that are high for this type of materials. This is a direct consequence of the designed polymeric structures, which have high DBD. In accordance with the observations from photo-DSC regarding

https://doi.org/10.1021/acsomega.3c02808
ACS Omega 2023, 8, 31009−31020

Table 4. DMA and TGA Data of the Printed Materials

Sample	DBD (mmol/g)	tan δ (°C)	cross-linking density (*10^3 mol/m^3)	E'@25 °C (MPa)	$T_{5\%}$ (°C)	T_{max} (°C)	residual mass@700 °C (%)
3D-SebA-47	4.88	105	1.22	340 ± 20	274.8	375.6	12.5
3D-SebA-37	4.48	93	2.44	410 ± 20	285.8	389.5	14.9
3D-SebA-27	4.08	85	3.22	340 ± 10	277.7	382	13.9
3D-IsA-47	4.98	118	1.01	300 ± 80	278.3	374.4	13.3
3D-IsA-37	4.6	110	2.10	660 ± 30	275.5	381	17.5
3D-IsA-27	4.22	103	2.41	560 ± 65	258.8	375	16.2
3D-SA-47	5.08	113	1.50	375 ± 55	278.5	381.2	13.3
3D-SA-37	4.72	109	3.22	465 ± 75	278.2	373.3	15.6
3D-SA-27	4.36	100	3.75	465 ± 15	294	364.7	16
3D-FDCA-47	4.98	110	1.44	545 ± 65	270	368.5	13.2
3D-FDCA-37	4.6	102	1.88	495 ± 25	281	364.5	17.5
3D-FDCA-27	4.22	91	2.14	385 ± 35	279.5	361.5	15.2
3D-PhA-47	4.98	110	1.48	420 ± 10	286.2	377	14.5
3D-PhA-37	4.6	110	1.67	575 ± 55	298.2	367.3	18.8
3D-PhA-27	4.22	100	2.03	585 ± 25	304.2	366	16.6

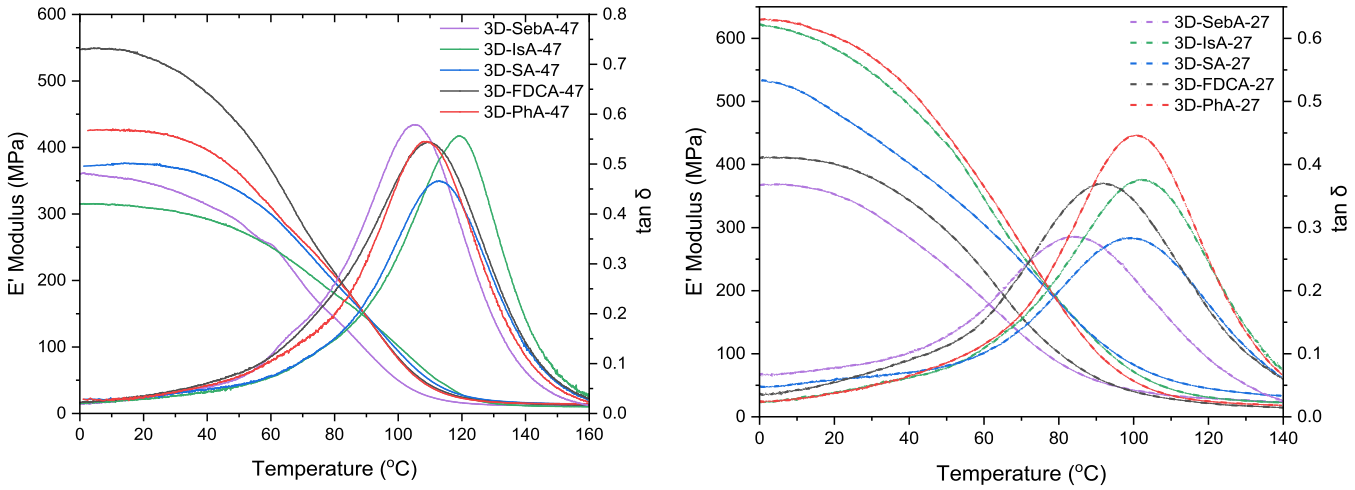

Figure 11. E' modulus and tan δ of the printed materials with 47 and 27% ACMO content.

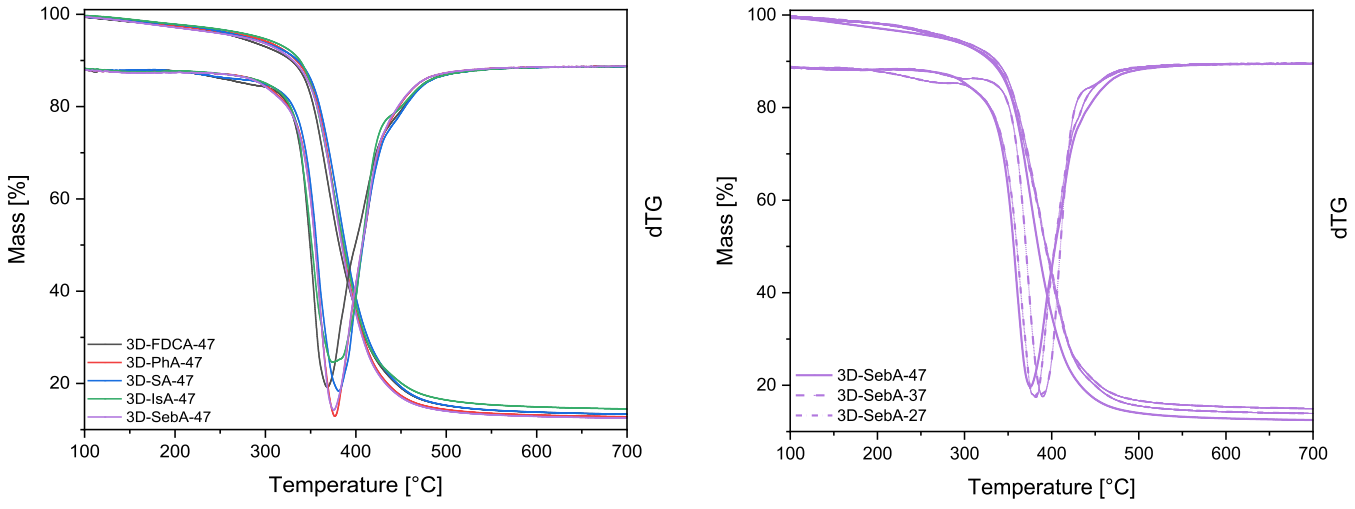

Figure 12. TGA results of the printed materials.

the C═C conversion, limiting the amount of ACMO in formulations from 47 to 37% increased the E' modulus significantly, while the further reduction of ACMO to 27% resulted in a slightly reduced E' modulus compared to the material with 37% ACMO, but still higher than the material with 47% ACMO. As conversions of the C═C increase, a denser cross-link network is created, as indicated by the calculated cross-linking densities in Table 4. However, the tan δ does not follow the same trend. As more polyester segments are incorporated in the network, which are "softer"

https://doi.org/10.1021/acsomega.3c02808
ACS Omega 2023, 8, 31009−31020

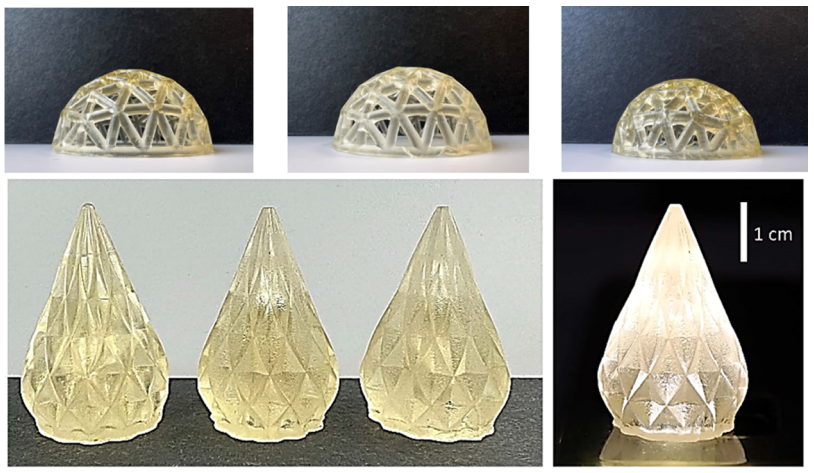

Figure 13. Upper row: printed domes utilizing formulations Form-SA-47, Form-SA-37, and Form-SA-27 (from left to right). Bottom left: 3D-printed "crystal sculptures" utilizing formulations Form-SA-47, Form-SA-37, and Form-SA-27 (from left to right). Bottom right: Form-SA-37 "crystal sculpture" illuminated from below.

compared to the cyclic ACMO structure, the network's flexibility increases, and this is reflected both in the reduction of E' modulus from materials with 37−27% diluent and in the lower tan δ values. Also, the tan δ peaks get broader with the reduction of ACMO, suggesting lower homogeneity in the network and therefore supporting the abovementioned claim.

Finally, in Figure 11, we present the DMA data from materials with 47 and 27% ACMO. The effect of the polyester structure is visible for materials with 27% ACMO, with aromatic structures presenting higher glass-transition temperatures and E' modulus compared to the aliphatic ones. On the contrary, when 47% of ACMO is used, no such relationship can be observed, as the reactive diluent structure seems to dominate the properties of the printed material. This is further evidence of the increased polyester segments in the network that was suggested before. The data of the formulations containing 37% ACMO are presented in the Supporting Information.

TGA. The thermal stability of the printed materials was examined with TGA measurements. Results for materials containing 47% ACMO are shown in Figure 12, along with the data for materials derived from PE-SebA. The rest of the results are reported in Figure S5 in the Supporting Information. Materials containing the same amount of ACMO present similar behavior, including a single degradation step and similar residual mass, as presented in Table 4. More pronounced differences can be found for materials derived from the same polyester but containing different amounts of reactive diluent. Limiting the amount of ACMO from 47 to 37% increased the thermal stability of the materials and the residual mass at 700 °C. This is in accordance with the findings from the DMA section, as these materials were found to contain a denser cross-linking network, which explains a superior thermal stability. Further reducing the diluent to 27% slightly deteriorated the thermal stability of the materials, but in most cases, results were similar or slightly better than those of the materials with 47% ACMO. All printed samples have a $T_{d5\%}$ above 250 °C, proving their suitability for a variety of applications.

CONCLUSIONS

This study was performed to elucidate the role of the reactive diluent concentration in formulations comprised of itaconic acid-based unsaturated polyester resins. Besides improving processability, by lowering the viscosity and increasing the reactivity toward UV-light-induced cross-linking, the diluent content was found to have a significant influence on the properties of the specimen obtained by means of additive manufacturing. Photo-DSC studies revealed that by increasing the diluent content, the rate of polymerization is also increased, while the overall conversion of reactive double bonds is reduced. RT-ATR verified that the diluent conversion is slower at lower concentrations of the diluent. The behavior toward UV light irradiation of each formulation type is also transferred to the properties of 3D-printed objects. A faster polymerization rate with lower conversions resulted in cross-linked materials of inferior thermomechanical performance, compared to materials with higher conversions. Out of the three different diluent contents that were tested during the course of the study, formulations with 37% of ACMO were found with the most promising combination of processability, reactivity, and thermomechanical response of their fabricated objects. We are therefore convinced that these materials can make a significant contribution to the field of bio-based UV-curing materials and in turn more sustainable additive manufacturing processes.

ASSOCIATED CONTENT

Supporting Information

The Supporting Information is available free of charge at https://pubs.acs.org/doi/10.1021/acsomega.3c02808.

Detailed description of the NMR data and figures of the photo-DSC, photorheology, real-time FTIR, DMA, and TGA measurements of all the formulations. (PDF)

AUTHOR INFORMATION

Corresponding Authors

Dimitrios N. Bikiaris − *Laboratory of Polymer Chemistry and Technology, Department of Chemistry, Aristotle University of Thessaloniki, GR-541 24 Thessaloniki, Greece;* orcid.org/0000-0001-8458-4952; Email: dbic@chem.auth.gr

https://doi.org/10.1021/acsomega.3c02808
ACS Omega 2023, 8, 31009−31020

Tobias Robert − *Fraunhofer Institute for Wood Research—Wilhelm-Klauditz-Institut WKI, 38108 Braunschweig, Germany*; orcid.org/0000-0002-6530-9741; Email: tobias.robert@wki.fraunhofer.de

Authors

Lazaros Papadopoulos − *Laboratory of Polymer Chemistry and Technology, Department of Chemistry, Aristotle University of Thessaloniki, GR-541 24 Thessaloniki, Greece*

Lorenzo Pezzana − *Dipartimento Scienza Applicata e Tecnologia, Politecnico di Torino, 10129 Torino, Italy*

Natalia Maria Malitowski − *Fraunhofer Institute for Wood Research—Wilhelm-Klauditz-Institut WKI, 38108 Braunschweig, Germany*

Marco Sangermano − *Dipartimento Scienza Applicata e Tecnologia, Politecnico di Torino, 10129 Torino, Italy*; orcid.org/0000-0002-8630-1802

Complete contact information is available at: https://pubs.acs.org/10.1021/acsomega.3c02808

Notes

The authors declare no competing financial interest.

■ ACKNOWLEDGMENTS

The research work was supported by the Hellenic Foundation for Research and Innovation (HFRI) under the 3rd Call for HFRI PhD Fellowships (Fellowship Number: 6186). This publication is based upon work from COST ActionFUR4Sustain, CA18220, supported by COST (European Cooperation in Science and Technology). The authors would like to thank Anja Gohla, Kirsten Wittenberg, and Dr. Alexandra Zamboulis for their help with TGA, viscosity, and NMR measurements.

■ REFERENCES

(1) MacArthur, D. E.; Waughray, D.; Stuchtey, M. R. The New Plastics Economy_Rethinking the Future of Plastics. In *World Economic Forum*; Ellen Macarthur Foundation: London, UK, 2016.

(2) Thompson, R. C.; Swan, S. H.; Moore, C. J.; vom Saal, F. S. Our Plastic Age. *Philos. Trans. R. Soc., B* **2009**, *364*, 1973−1976.

(3) Schneiderman, D. K.; Hillmyer, M. A. 50th Anniversary Perspective: There Is a Great Future in Sustainable Polymers. *Macromolecules* **2017**, *50*, 3733−3749.

(4) Werpy, T.; Petersen, G. *Top Value Added Chemicals from Biomass: Volume I—Results of Screening for Potential Candidates from Sugars and Synthesis Gas*; Golden: CO, United States, 2004. DOI: 10.2172/15008859.

(5) Willke, T.; Vorlop, K. D. Biotechnological Production of Itaconic Acid. *Appl. Microbiol. Biotechnol.* **2001**, *56*, 289−295.

(6) Krull, S.; Lünsmann, M.; Prüße, U.; Kuenz, A. Ustilago Rabenhorstiana—An Alternative Natural Itaconic Acid Producer. *Fermentation* **2020**, *24*, 1−16.

(7) Saha, B. C.; Kennedy, G. J. Phosphate Limitation Alleviates the Inhibitory Effect of Manganese on Itaconic Acid Production by *Aspergillus terreus*. *Biocatal. Agric. Biotechnol.* **2019**, *18*, No. 101016.

(8) Melilli, G.; Guigo, N.; Robert, T.; Sbirrazzuoli, N. Radical Oxidation of Itaconic Acid-Derived Unsaturated Polyesters under Thermal Curing Conditions. *Macromolecules* **2022**, *55*, 9011−9021.

(9) Mehta, L. B.; Wadgaonkar, K. K.; Jagtap, R. N. Synthesis and Characterization of High Bio-Based Content Unsaturated Polyester Resin for Wood Coating from Itaconic Acid: Effect of Various Reactive Diluents as an Alternative to Styrene. *J. Dispersion Sci. Technol.* **2019**, *40*, 756−765.

(10) Li, Q.; Ma, S.; Xu, X.; Zhu, J. Bio-Based Unsaturated Polyesters. In *Unsaturated Polyester Resins*; Elsevier, 2019; pp 515−555. DOI: 10.1016/B978-0-12-816129-6.00020-X.

(11) Panic, V. V.; Seslija, S. I.; Popovic, I. G.; Spasojevic, V. D.; Popovic, A. R.; Nikolic, V. B.; Spasojevic, P. M. Simple One-Pot Synthesis of Fully Biobased Unsaturated Polyester Resins Based on Itaconic Acid. *Biomacromolecules* **2017**, *18*, 3881−3891.

(12) Fidanovski, B. Z.; Spasojevic, P. M.; Panic, V. V.; Seslija, S. I.; Spasojevic, J. P.; Popovic, I. G. Synthesis and Characterization of Fully Bio-Based Unsaturated Polyester Resins. *J. Mater. Sci.* **2018**, *53*, 4635−4644.

(13) Robert, T.; Friebel, S. Itaconic Acid-a Versatile Building Block for Renewable Polyesters with Enhanced Functionality. *Green Chem.* **2016**, *18*, 2922−2934.

(14) Suriano, R.; Gonzalez, M. N. G.; Turri, S. Environmental Profile and Technological Validation of New High-Tg Unsaturated Polyesters from Fully Bio-Based Monomers and Reactive Diluents. *J. Polym. Environ.* **2021**, *29*, 1122−1133.

(15) López-Carrasquero, F.; Martínez de Ilarduya, A.; Cárdenas, M.; Carrillo, M.; Luisa Arnal, M.; Laredo, E.; Torres, C.; Méndez, B.; Müller, A. J. New Comb-like Poly(n-Alkyl Itaconate)s with Crystalizable Side Chains. *Polymer* **2003**, *44*, 4969−4979.

(16) Arrighi, V.; McEwen, I. J.; Holmes, P. F. Dielectric Relaxations in Poly(Di- n -Alkyl Itaconate)s. *Macromolecules* **2004**, *37*, 6210−6218.

(17) Sollka, L.; Lienkamp, K. Progress in the Free and Controlled Radical Homo- and Co-Polymerization of Itaconic Acid Derivatives: Toward Functional Polymers with Controlled Molar Mass Distribution and Architecture. *Macromol. Rapid Commun.* **2021**, *42*, No. 2000546.

(18) Li, P.; Ma, S.; Dai, J.; Liu, X.; Jiang, Y.; Wang, S.; Wei, J.; Chen, J.; Zhu, J. Itaconic Acid as a Green Alternative to Acrylic Acid for Producing a Soybean Oil-Based Thermoset: Synthesis and Properties. *ACS Sustainable Chem. Eng.* **2017**, *5*, 1228−1236.

(19) Pérocheau Arnaud, S.; Andreou, E.; Pereira Köster, L. V. G.; Robert, T. Selective Synthesis of Monoesters of Itaconic Acid with Broad Substrate Scope: Biobased Alternatives to Acrylic Acid. *ACS Sustainable Chem. Eng.* **2020**, *8*, 1583−1590.

(20) Farmer, T. J.; Comerford, J. W.; Pellis, A.; Robert, T. Post-Polymerization Modification of Bio-Based Polymers: Maximizing the High Functionality of Polymers Derived from Biomass. *Polym. Int.* **2018**, *67*, 775−789.

(21) Brännström, S.; Malmström, E.; Johansson, M. Biobased UV-Curable Coatings Based on Itaconic Acid. *J. Coat. Technol. Res.* **2017**, *14*, 851−861.

(22) Robert, T.; Eschig, S.; Biemans, T.; Scheifler, F. Bio-Based Polyester Itaconates as Binder Resins for UV-Curing Offset Printing Inks. *J. Coat. Technol. Res.* **2019**, *16*, 689−697.

(23) Maturi, M.; Pulignani, C.; Locatelli, E.; Vetri Buratti, V.; Tortorella, S.; Sambri, L.; Comes Franchini, M. Phosphorescent Bio-Based Resin for Digital Light Processing (DLP) 3D-Printing. *Green Chem.* **2020**, *22*, 6212−6224.

(24) Vetri Buratti, V.; Sanz De Leon, A.; Maturi, M.; Sambri, L.; Molina, S. I.; Comes Franchini, M. Itaconic-Acid-Based Sustainable Poly(Ester Amide) Resin for Stereolithography. *Macromolecules* **2022**, *55*, 3087−3095.

(25) Miao, J.-T.; Peng, S.; Ge, M.; Li, Y.; Zhong, J.; Weng, Z.; Wu, L.; Zheng, L. Three-Dimensional Printing Fully Biobased Heat-Resistant Photoactive Acrylates from Aliphatic Biomass. *ACS Sustainable Chem. Eng.* **2020**, *8*, 9415−9424.

(26) Barkane, A.; Jurinovs, M.; Briede, S.; Platnieks, O.; Onufrijevs, P.; Zelca, Z.; Gaidukovs, S. Biobased Resin for Sustainable Stereolithography: 3D Printed Vegetable Oil Acrylate Reinforced with Ultra-Low Content of Nanocellulose for Fossil Resin Substitution. *3D Print. Addit. Manuf.* **2022**, No. 0294.

(27) Barkane, A.; Platnieks, O.; Jurinovs, M.; Kasetaite, S.; Ostrauskaite, J.; Gaidukovs, S.; Habibi, Y. UV-Light Curing of 3D Printing Inks from Vegetable Oils for Stereolithography. *Polymers* **2021**, *13*, 1195.

(28) Chyr, G.; DeSimone, J. M. Review of High-Performance Sustainable Polymers in Additive Manufacturing. *Green Chem.* **2023**, *25*, 453−466.

(29) Guggenbiller, G.; Brooks, S.; King, O.; Constant, E.; Merckle, D.; Weems, A. C. 3D Printing of Green and Renewable Polymeric Materials: Toward Greener Additive Manufacturing. *ACS Appl. Polym. Mater.* **2023**, *5*, 3201−3229.
(30) Maines, E. M.; Porwal, M. K.; Ellison, C. J.; Reineke, T. M. Sustainable Advances in SLA/DLP 3D Printing Materials and Processes. *Green Chem.* **2021**, *23*, 6863−6897.
(31) Papadopoulos, L.; Malitowski, N. M.; Bikiaris, D.; Robert, T. Bio-Based Additive Manufacturing Materials: An in-Depth Structure-Property Relationship Study of UV-Curing Polyesters from Itaconic Acid. *Eur. Polym. J.* **2023**, *186*, No. 111872.
(32) Pérocheau Arnaud, S.; Malitowski, N. M.; Meza Casamayor, K.; Robert, T. Itaconic Acid-Based Reactive Diluents for Renewable and Acrylate-Free UV-Curing Additive Manufacturing Materials. *ACS Sustainable Chem. Eng.* **2021**, *9*, 17142−17151.
(33) Murayama, T.; Bell, J. P. Relation between the Network Structure and Dynamic Mechanical Properties of a Typical Amine-Cured Epoxy Polymer. *J. Polym. Sci., Part A-2: Polym. Chem.* **1970**, *8*, 437−445.
(34) Papadopoulos, L.; Kluge, M.; Bikiaris, D. N.; Robert, T. Straightforward Synthetic Protocol to Bio-Based Unsaturated Poly-(Ester Amide)s from Itaconic Acid with Thixotropic Behavior. *Polymers.* **2020**, *12*, 980.
(35) Harikrishna, R.; Ponrathnam, S.; Rajan, C. R.; Tambe, S. S. Photopolymerization of Bis-Aromatic and Alicyclic Based Solid Urethane Acrylate Macromonomer in the Presence of Large Excess of Reactive Diluent: Kinetics and Modeling. *J. Therm. Anal. Calorim.* **2013**, *112*, 805−813.
(36) Gorsche, C.; Harikrishna, R.; Baudis, S.; Knaack, P.; Husar, B.; Laeuger, J.; Hoffmann, H.; Liska, R. Real Time-NIR/MIR-Photorheology: A Versatile Tool for the in Situ Characterization of Photopolymerization Reactions. *Anal. Chem.* **2017**, *89*, 4958−4968.
(37) Mojon, P.; Oberholzer, J.-P.; Meyer, J.-M.; Belser, U. C. Polymerization Shrinkage of Index and Pattern Acrylic Resins. *J. Prosthet. Dent.* **1990**, *64*, 684−688.
(38) Pezzana, L.; Wolff, R.; Melilli, G.; Guigo, N.; Sbirrazzuoli, N.; Stampfl, J.; Liska, R.; Sangermano, M. Hot-Lithography 3D Printing of Biobased Epoxy Resins. *Polymer* **2022**, *254*, No. 125097.
(39) Dall'Argine, C.; Hochwallner, A.; Klikovits, N.; Liska, R.; Stampf, J.; Sangermano, M. Hot-Lithography SLA-3D Printing of Epoxy Resin. *Macromol. Mater. Eng.* **2020**, *305*, No. 2000325.

https://doi.org/10.1021/acsomega.3c02808
ACS Omega 2023, 8, 31009−31020